Available online at www.sciencedirect.com
SCIENCE DIRECT®
ELSEVIER
Journal of Magnetism and Magnetic Materials 297 (2006) 76–83
Journal of magnetism and magnetic materials
www.elsevier.com/locate/jmmm

High-performance zig-zag and meander inductors embedded in ferrite material

Goran Stojanovic[a,*], Mirjana Damnjanovic[a], Vladan Desnica[a], Ljiljana Zivanov[a], Ramesh Raghavendra[b], Pat Bellew[b], Neil Mcloughlin[b]

[a]*Faculty of Technical Sciences, Department of Electronics, University of Novi Sad, Trg Dositeja Obradovica 6, Novi Sad 21000, Serbia and Montenegro*
[b]*Littelfuse Ireland Limited, Ecco Road, Dundalk, Co. Louth, Ireland*

Received 29 December 2004; received in revised form 11 February 2005
Available online 16 March 2005

Abstract

This paper describes the design, modeling, simulation and fabrication of zig-zag and meander inductors embedded in low- or high-permeability soft ferrite material. These microinductors have been developed with ceramic coprocessing technology. We compare the electrical properties of zig-zag and meander inductors structures installed as surface-mount devices. The equivalent model of the new structures is presented, suitable for design, circuit simulations and for prediction of the performance of proposed inductors. The relatively high impedance values allow these microinductors to be used in high-frequency suppressors. The components were tested in the frequency range of 1 MHz–3 GHz using an Agilent 4287A RF LCR meter. The measurements confirm the validity of the analytical model.

PACS: 84.32.Hh

Keywords: Inductor; High frequency; Surface-mounted devices; Soft ferrite

1. Introduction

Miniature inductors embedded in a high- or low-permeability soft ferrite material, find useful application in the suppression of EMI at RF microwave frequencies. Their size, performance and reliability make them very attractive for a wide range of applications, such as electromagnetic interference (EMI) suppression in universal series bus (USB), low-voltage differential signaling and in other high-speed digital interfaces incorporated in notebooks and personal computers, digital cameras and scanners.

Planar magnetic components are suitable because of their small size. This is a direct

*Corresponding author. Tel.: +381 21 459 449; fax: +381 21 475 0572.
E-mail addresses: sgoran@uns.ns.ac.yu (G. Stojanovic), rraghavendra@littlefuse.com (R. Raghavendra).

0304-8853/$ - see front matter © 2005 Elsevier B.V. All rights reserved.
doi:10.1016/j.jmmm.2005.02.058

manifestation of the general principle that the size of magnetic components is reduced as frequency increases. Unfortunately, high-frequency operation gives rise to unwanted skin effect and proximity effect losses. In recent years much literature [1–8] has studied the high-frequency characteristics of ferrite core and/or magnetic components such as ferrite inductors, based on finite element method or physical analysis.

Miniature inductors can be installed as surface-mount devices (SMDs) [9]. Parasitic effects such as stray capacitance, self-resonance and magnetic losses of ferrite, etc., play an important role in the design of such inductors. An understanding of the high-frequency parasitic and packaging effects can be gained from equivalent circuit description of the inductor.

The momentum towards high-density electronic circuits continues unabated. The effects are obvious in very large scale integration (VLSI) design: component densities are being quadrupled every three years. Planar magnetic components can become an integral part of the process, whereby resistors and capacitors are already established components. One of the major drawbacks in establishing planar magnetic technology is the lack of accurate analytical models for different types of these structures. Experimental prototypes are expensive to fabricate and test. One would normally expect to complete a second cycle of fabrication and testing before a final design is achieved. While this procedure may give better insight, it does not lead to an established design methodology.

The purpose of this paper is to address this situation. In many applications, it is required to design miniature inductors with resonant frequency extending into the RF regime (100 MHz–1 GHz). Thus, there is a pressing need to understand the full circuit modeling and characterization of the miniature inductor, including the circuit parasitic and the material effects mentioned above.

2. Inductor structures and description of calculation techniques

The proposed zig-zag and meander structures are realized as SMDs for the typical 0805 chip size, and labels of mechanical dimensions of the chip are shown in Fig. 1 (for chip size 0805 mechanical dimensions are $D = 1.1\,\text{mm}$, $E = 0.25\,\text{mm} \pm 0.075$, $L = 2.01\,\text{mm} \pm 0.2$, $W = 1.25\,\text{mm} \pm 0.20$). Fig. 2 shows the cross-section of fabricated zig-zag and meander inductors embedded in ferrite material. The components were fabricated using the ceramic coprocessing technology. The conductive layer, platinum, Pt ($\rho = 10.6 \times 10^{-8}\,\Omega\,\text{m}$) with the lower electric resistivity was chosen as the conductor to form inductors. The width of the conductor is 150 μm and the thickness of the conductive layer is 10 μm. The microinductor is embedded in the middle of a ferrite layer. The ferrite materials have remarks as LP (*low-permeability ferrite material*) and HP (*high-permeability ferrite material*), whose characteristics are available commercially from Neosid [10], Hereaus, Ferro, etc. LP nickel–zinc ferrite has low loss factors at medium frequencies and high suppression impedance at high frequencies (over 100 MHz). HP ferrite material is nickel–zinc ferrite, with initial permeability 1000 (while LP has initial permeability 220). These ferrite materials find typical applications in EMI suppression components.

In order to analyze zig-zag and meander inductors embedded in ferrite material, the equivalent circuit describing electrical properties of the presented structure is determined, and is depicted in Fig. 3. Resistances R_w and R_f are the winding and ferrite resistances, respectively. The element R_{DCT} presents the total DC resistance. Inductance

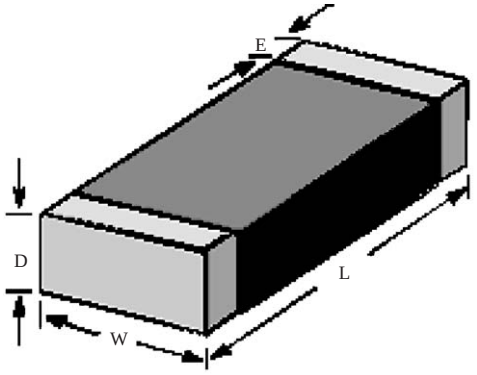

Fig. 1. Label of mechanical dimensions of inductor SMD packages.

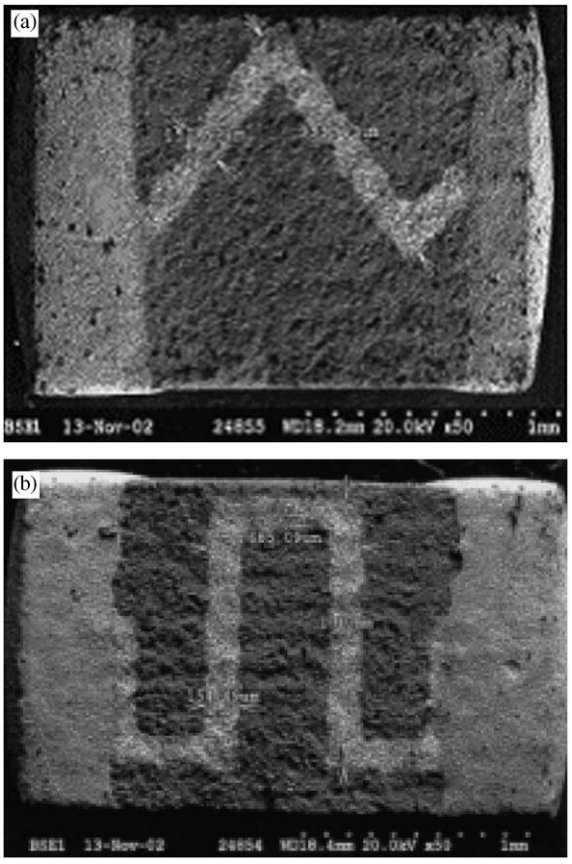

Fig. 2. (a) Zig-zag inductor and (b) meander inductor embedded in ferrite material.

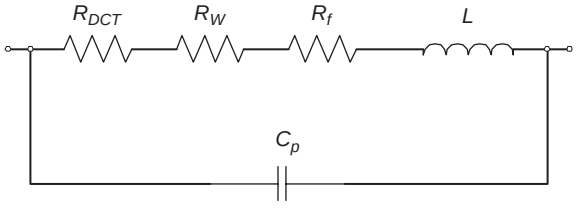

Fig. 3. The lumped parameter equivalent circuit of an inductor embedded in ferrite.

L is the frequency dependent inductance of the inductor and C_p is the overall parasitic capacitance including the distributed turn-to-turn and turn-to-ferrite stray capacitance. The useful operating frequency range of the inductor is thus limited by its self-resonant frequency.

The permeability of the ferrite material is a complex parameter consisting of a real μ'_r and imaginary part μ''_r,

$$\mu_r(f) = \mu'_r(f) - j\mu''_r(f). \quad (1)$$

The real component represents the reactive portion of impedance, and the imaginary component represents the losses. Both parts of the permeability are frequency dependent, as can be seen in Ref. [10]. The analytical expressions for real $\mu'_r(f)$ and imaginary part $\mu''_r(f)$ are obtained using fitting techniques according to measurement (data, which are derived from measurements on toroidal cores and the values obtained in Ref. [10], cannot be directly transferred to products of another shape and size). Simulations of zig-zag and meander inductors embedded in ferrite materials were performed using our software tool—SPIS^{TM} (Simulator for Planar Inductive Structures) based on the calculation method described briefly in this subsection.

2.1. Inductance calculation

The calculation of electrical parameters (inductance, resistance, impedance, Q-factor) of zig-zag or meander inductors is very complex. Therefore, the inductor is divided into segments having small, rectangular cross sections. To obtain the correct total inductance L, the mutual inductance M between all segments of the inductor has to be calculated and added to the sum of all segments self- inductance L_S [11]. The total inductance L is

$$L = \sum L_S - \sum |M^-| + \sum M^+. \quad (2)$$

For a straight conductor of rectangular cross section, self-inductance is given by the following formula:

$$L_S(f) = \left(\frac{\mu_0 l}{2\pi}\right)\left(\mu'_r(f)\left(\ln\left(\frac{2l}{w+t}\right) + 0.25049 + \frac{(w+t)}{3l}\right) + \frac{T(f)}{4}\right), \quad (3)$$

where w is conductor width, t is conductor thickness, l is conductor length and $T(f)$ is a frequency-dependent factor. The computation concept considers segments as simple filaments

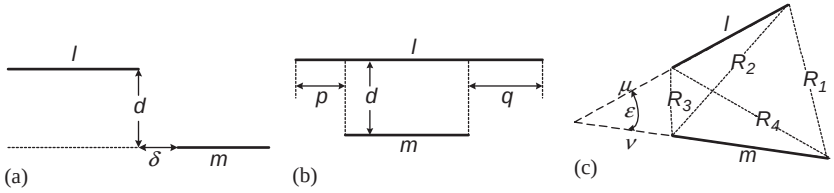

Fig. 4. The possible mutual position segments of zig-zag and meander inductors.

for the calculation of mutual inductance. Depending on the current vectors in segments (filaments), the mutual inductance is positive M^+ if the current vectors are in the same direction or negative M^- if the current vectors are in opposite directions. The possible configurations in space are illustrated in Fig. 4.

The mutual inductance of two parallel segments of equal length l, forming an orthogonal rectangle, is given by

$$M_l = 2lU = 2l\ln\{(l/\mathrm{GMD}) + [1 + (l^2/\mathrm{GMD}^2)]^{1/2}\} - [1 + (\mathrm{GMD}^2/l^2)]^{1/2} + (\mathrm{GMD}/l). \tag{4}$$

All other configurations of parallel segments are based on this equation. Attention should be paid to the U factor in the equation above. U is calculated using closed-form expressions provided in the open literature, and concerns the various cases of the geometric mean distance (GMD) between two conductors of width w and thickness t, separated by d. The concept of GMD may be used for parallel segments, which are coupled most strongly. Mutual inductance parameter U is calculated from the equation above, where GMD is given:

$$\ln \mathrm{GMD} = \ln d - \left\{\left[\tfrac{1}{12}(d/w)^2\right] + \left[\tfrac{1}{60}(d/w)^4\right] + \left[\tfrac{1}{168}(d/w)^6\right] + \left[\tfrac{1}{360}(d/w)^8\right] + \left[\tfrac{1}{660}(d/w)^{10}\right] + \cdots\right\}. \tag{5}$$

When the segments are parallel, two distinct cases may appear. The first is shown in Fig. 4(a) and the mutual inductance is calculated by

$$2M = (M_{l+m\pm\delta} + M_\delta) - (M_{l\pm\delta} + M_{m\pm\delta}), \tag{6}$$

where δ is positive for non-overlapping segments and negative for overlapping ones. In the second case as shown in Fig. 4(b), the mutual inductance between the two conductors with lengths l and m is calculated by

$$2M = (M_{m+p} + M_{m+q}) - (M_p + M_q). \tag{7}$$

The mutual inductance of two straight segments (filaments) have lengths l and m and when produced to their point of intersection the latter is distant from their nearer ends by distances μ and ν, respectively. The four distances between the ends of the filaments are as shown in Fig. 4(c). The formula for the mutual inductance is given by [12]

$$M = \frac{\mu_0\mu_r}{4\pi}\cos\varepsilon\left[(\mu + l)\,\mathrm{arth}\frac{m}{R_1 + R_2} + (\nu + m)\,\mathrm{arth} \times \frac{l}{R_1 + R_4} - \mu\,\mathrm{arth}\frac{m}{R_3 + R_4} - \nu\,\mathrm{arth}\frac{l}{R_2 + R_3}\right]. \tag{8}$$

In Eq. (8) $\cos\varepsilon$, μ, and ν are

$$\cos\varepsilon = \frac{\alpha^2}{2lm}, \quad \text{where } \alpha^2 = R_4^2 - R_3^2 + R_2^2 - R_1^2, \tag{9}$$

$$\mu = \frac{\left[2m^2\left(R_2^2 - R_3^2 - l^2\right) + \alpha^2\left(R_4^2 - R_3^2 - m^2\right)\right]l}{4l^2m^2 - \alpha^4},$$
$$\nu = \frac{\left[2l^2\left(R_4^2 - R_3^2 - m^2\right) + \alpha^2\left(R_2^2 - R_3^2 - l^2\right)\right]m}{4l^2m^2 - \alpha^4}, \tag{10}$$

and $R_1 = R(m, l, \mu, \nu)$, $R_2 = R(0, l, \mu, \nu)$, $R_3 = R(0, 0, \mu, \nu)$, $R_4 = R(m, 0, \mu, \nu)$, where

$$R(x, y, \mu, \nu) = \sqrt{(\mu + y)^2 + (\nu + x)^2 - 2(\mu + y)(\nu + x)\cos\varepsilon}. \tag{11}$$

2.2. Resistance calculation

The total resistance R is the sum of total DC resistance R_{DCT}, winding resistance R_w and ferrite resistance R_f (all parameters are shown in Fig. 3). Therefore, R can be expressed as:

$$R = R_{DCT} + R_w + R_f. \tag{12}$$

The total DC resistance is several times larger (due to the resistance of the contacts) than the resistance calculated by

$$R_{DC} = \rho \frac{l}{wt}, \tag{13}$$

where ρ is the resistivity of the Pt conductor layer of thickness t, width w and length l.

The resistance of an inductor increases with frequency because of skin and proximity effects due to the time-varying electromagnetic field. The final result of these two combined effects is a reduction in the effective cross-sectional area of the conductive material available for the current flow. Therefore, the AC resistance (or winding resistance) at high frequencies becomes greater than the DC resistance [1]:

$$R_w = R_{DC} A \left[\frac{e^{2A} - e^{-2A} + 2\sin(2A)}{e^{2A} + e^{-2A} - 2\cos(2A)} + 2\,\frac{N_i^2 - 1}{3}\,\frac{e^{A} - e^{-A} - 2\sin(A)}{e^{A} + e^{-A} + 2\cos(A)} \right], \tag{14}$$

where A is a factor which depends on winding geometry. The first and second terms represent the skin effect and proximity effect in the winding, respectively. For a strip wire, having conductors with dimensions w and t, A becomes $A = (w/\delta)\sqrt{t/p}$, where p is the distance between the centers of two adjacent conductors ($p \approx t$ for right conductor segment) and δ is the skin depth of wire expressed as $\delta = \sqrt{\rho/\pi\mu_0\mu_{rw}f}$.

The lumped parameter R_f from Fig. 3 is given by

$$R_f = 2\pi f L_0 \mu_r'', \tag{15}$$

where f is frequency, L_0 is the inductance of inductor in vacuum environment and μ_r'' is the imaginary part of complex permeability.

2.3. Capacitance calculation

Expression for parasitic capacitance (element of equivalent model in Fig. 3) is

$$C_p = l_{tot}\left[\varepsilon_0\varepsilon_r \frac{2\pi}{\ln(1 + 2h/t + \sqrt{2h/t(2h/t+2)})} + \varepsilon_0\varepsilon_r \frac{w - t/2}{h} \right], \tag{16}$$

where l_{tot} is the total length of conductor segments, t the thickness of conductor, w the width of conductor, $h = 0.5^*$ (width of ferrite layer).

2.4. Impedance calculation

As impedance consists of a reactive and a resistive part, in order to represent this, permeability should have two parts, too. The real part corresponds to the reactance, positive for an inductance, negative for a capacitance, and the imaginary part to the losses. Thus, the formula for impedance can be given as

$$|Z| = \sqrt{R^2 + (2\pi f \mu' L_0)^2}. \tag{17}$$

2.5. Quality factor calculation

For an equivalent circuit of proposed structures, as in Fig. 3, the quality factor is

$$Q = \frac{\mathrm{Im}(Z)}{\mathrm{Re}(Z)} = \frac{\omega L}{R}(1 - \omega^2 L C_p) - \omega R C_p. \tag{18}$$

The proposed model allows accurate prediction of all the parameters affecting the zig-zag and meander inductors embedded in ferrite materials, as well as their control during the design process.

3. Results and discussion

The measurement and characterization of the components have been performed using an Agilent 4287A RF LCR meter for frequencies up to 3 GHz.

Electrical characterization data obtained for zig-zag and meander inductors embedded in LP ferrite

material are shown in Figs. 5 and 6. For LP ferrite material, we are given measured data only for a zig-zag inductor. Simulation of the zig-zag and meander inductor embedded in soft ferrite material was done using our software tool SPIS^{TM}, based on the calculation method described in a previous section.

The measured and calculated data obtained for zig-zag and meander inductors embedded in HP soft ferrite material are shown in Figs. 7 and 8.

The planar microinductors employed in this paper generate well-localized magnetic fields existing only in the vicinity of the inductor plane due to some kind of periodicity in the inductor. Therefore, the electromagnetic field is confined in sandwich structure, hence resulting in virtually no EMI to other low-energy level components in the electronic systems.

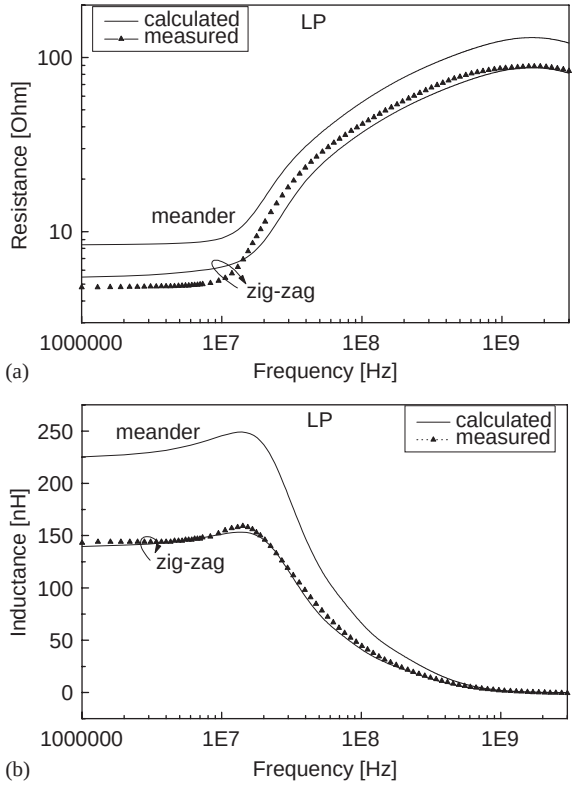

Fig. 5. For LP ferrite material (a) measured and calculated total resistance, (b) measured and calculated total inductance.

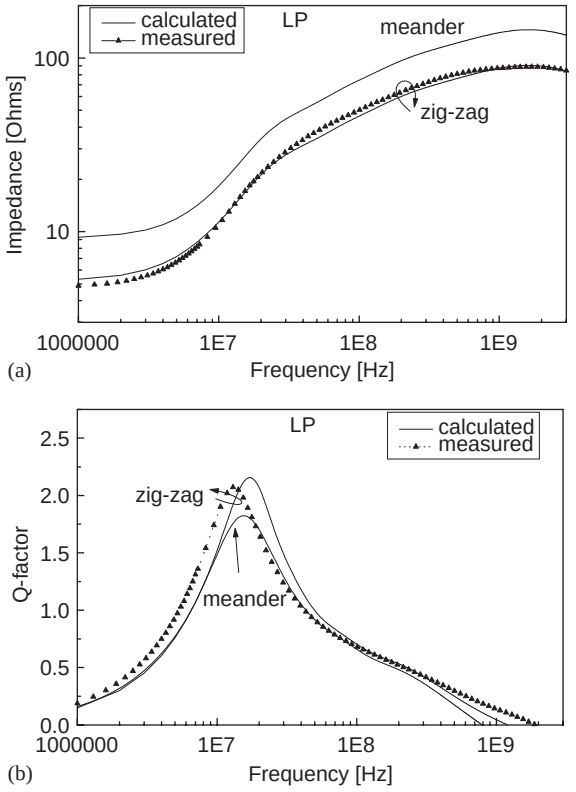

Fig. 6. For LP ferrite material (a) measured and calculated impedance, (b) measured and calculated quality factor.

The knowledge about the current distribution in a single rectangular conductor in elemental cases forms a base for understanding AC resistance of the conductor. The nature of the currents is that they flow to the part of the conductor where they see less impedance or inter-linkage flux. To immerse the conductor deep into the magnetic material is a good method to reduce the influence of the frequency magnetic field on the conductor losses.

Magnetic losses in the ferrite are predominantly due to an imaginary part of the permeability. At RF, these ferrite losses dominate the winding losses. It is emphasized that all circuit parameters are in general frequency-dependent, especially at RF, because the constitutive parameters of ferrite material are frequency-dependent.

At RF frequencies, the zig-zag and meander inductor embedded in the ferrite materials shows

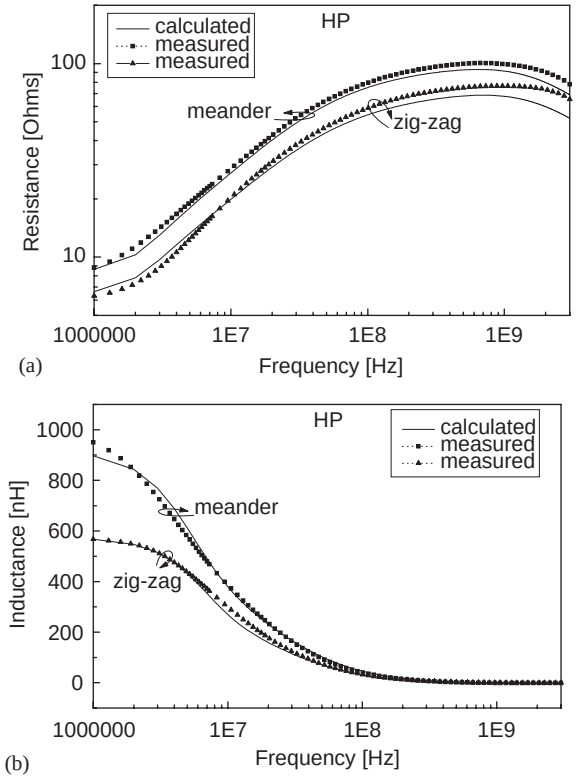

Fig. 7. For HP ferrite material (a) measured and calculated total resistance, (b) measured and calculated total inductance.

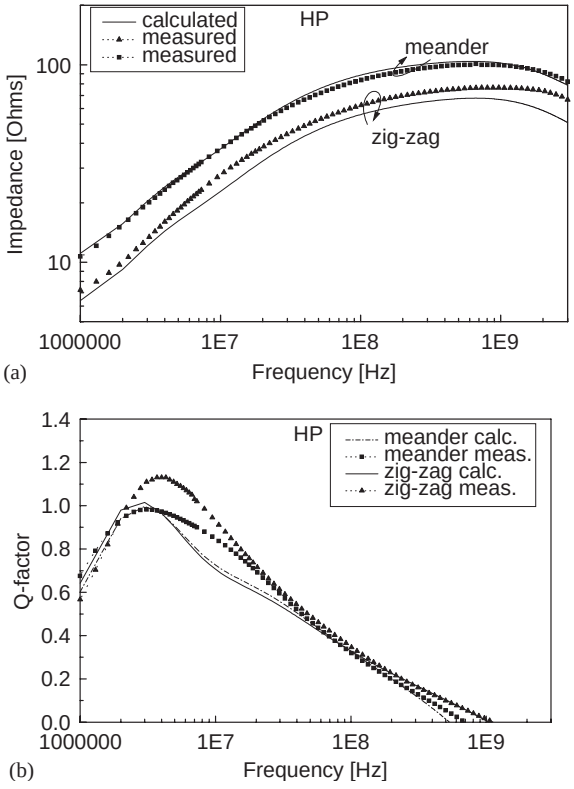

Fig. 8. For HP ferrite material (a) measured and calculated impedance, (b) measured and calculated quality factor.

high impedance, which suppresses unwanted interference. For HP material, the maximal of the impedance value is on some lower frequencies than LP ferrite material, thus lending the structure to usage in this frequency range. The inductance for the meander inductor is greater because a conductor line for the zig-zag inductor has no maximal possible length (within the mechanical dimensions of an SMD chip), and the inductance of the zig-zag inductor can be increased, if we increase the length of conductor segments and decrease the angle between two neighboring conductors.

To achieve even higher inductance, a few changes of the meander inductor structure can be made: the length of the conductor segment has to be maximal possible and/or the structure must have the maximal possible number of turns. If the meander inductor is designed to have more turns (if the distance between two neighboring conductors is equal to the conductor's width w), this will result in the greater total inductance (and impedance, also) of novel structures.

Cofiring of ceramics is not easy and is fraught with difficulty [13]. Material diffusion or contamination is a key concern when dealing with electrical properties [14]. The diffusion of Pt into ferrite materials can result in deterioration of both ferrite material characteristics and conductor material characteristics. It is not possible to include this phenomenon in the model successfully. Thus, the small deviation of the measurement results compared to the calculated ones can be a consequence of the above reasons. Although the analytical modeling of the inductors embedded in ferrite material is quite complex, our calculated responses are very close to measured results. The only measured response that does not track very well with calculated one is the Q-factor for inductors embedded in HP soft ferrite material.

This slight discrepancy can be explained by means of formula (18). The quality factor is quite complex (it depends on R, L and C_p and they depend on permeability). Thus, the small deviation of the measurement results compared to the calculated ones is a consequence of its complexity, and this deviation is greater in the case of a HP ferrite because its permeability is higher than LP ferrite.

4. Conclusion

In this paper, the design, modeling and fabrication of the zig-zag and meander inductor embedded in the LP and HP nickel–zinc ferrite materials have been discussed. The size of the chip considered structures is 0805 in SMD packages. As can be seen, the presented results enable the application of the proposed new components in EMI/EMC (electromagnetic interference/electromagnetic compatibility) suppression of induced and conductive EM noise in the secondary step of EMI suppression. An accurate description of the frequency response of the zig-zag and meander inductor is achieved by means of a simple equivalent circuit model. The model allows all parameters affecting the inductor electrical performance to be accurately predicted and controlled during the design process. Theoretical (calculated) plots of inductors resistance, inductance, impedance and quality factor have been drawn and compared with measured data. The results obtained by the proposed method are in very good agreement with measured data over the frequency range from 1 MHz to 3 GHz.

Acknowledgement

This work was supported by Littelfuse Ireland Limited, Dundalk, Ireland. The authors would like to acknowledge Littelfuse Ireland Limited for continuous support and understanding during the project.

References

[1] M.K. Kazimierczuk, G. Sancineto, G. Grandi, U. Reggiani, A. Massarini, IEEE Trans. Magn. 35 (1999) 4185.
[2] Q. Yu, T.W. Holmes, K. Naishadham, IEEE Trans. Electron. Comput. 44 (2002) 258.
[3] G. Grandi, M.K. Kazimierczuk, A. Massarini, U. Reggiani, G. Sancineto, IEEE Trans. Magn. 40 (2004) 1839.
[4] C.K. Liu, T.W. Law, P.L. Cheng, I.T. Chong, D.C.C. Lam, Electronic Components and Technology Conference, 2002, p. 490.
[5] A. Reatti, M.K. Kazimierczuk, IEEE Trans. Magn. 38 (2002) 1512.
[6] X.L. Tang, H.W. Zhang, H. Su, X.D. Jiang, J. Magn. Magn. Mater. 270 (2004) 84.
[7] H. Leiste, K. Seemann, V. Bekker, J. Magn. Magn. Mater. 272 (2004) e1135.
[8] E. Gamet, J.P. Chatelon, T. Rouiller, B. Bayard, G. Noyel, J.J. Rousseau, J. Magn. Magn. Mater. 288 (2005) 121.
[9] K. Naishadham, IEEE Trans. Electron. Comput. 43 (2001) 557.
[10] M.M.G. Neosid, available: http://www.mmggb.com/pdfs/mmg-Materials.pdf
[11] H.M. Greenhouse, IEEE Trans. Part. Hybr. Pack. PHP-10 (1974) 101.
[12] F.W. Grover, Inductance calculations working formulas and tables, Princeton, D. van Nostrand Comp., Inc., 1946 (reprinted by Dover, New York, 1954).
[13] A. Rafferty, Y. Gun'ko, R. Raghavendra, J. Eur. Ceram. Soc. 24 (2004) 2005.
[14] R. Raghavendra, P. Bellew, N. Mcloughlin, G. Stojanovic, M. Damnjanovic, V. Desnica, Lj. Zivanov, IEEE Electron. Devices Lett. 25 (2004) 778.